Journal of the Mechanical Behavior of Biomedical Materials 101 (2020) 103422

Contents lists available at ScienceDirect

Journal of the Mechanical Behavior of Biomedical Materials

journal homepage: www.elsevier.com/locate/jmbbm

Effects of mechanical injury on the tribological rehydration and lubrication of articular cartilage

Margot S. Farnham[a], Riley E. Larson[a], David L. Burris[a,b], Christopher Price[a,b,*]

[a] Department of Biomedical Engineering, University of Delaware, Newark, DE, USA
[b] Department of Mechanical Engineering, University of Delaware, Newark, DE, USA

ARTICLE INFO

Keywords:
Cartilage biomechanics and tribology
Post-traumatic osteoarthritis
Cartilage strain and friction
Impact injury
Cartilage fissures and chondral defects

ABSTRACT

Healthy articular cartilage is crucial to joint function, as it provides the low friction and load bearing surface necessary for joint articulation. Nonetheless, joint injury places patients at increased risk of experiencing both accelerated cartilage degeneration and wear, and joint dysfunction due to post-traumatic osteoarthritis (PTOA). In this study, we used our *ex vivo* convergent stationary contact area (cSCA) explant testing configuration to demonstrate that high-speed sliding of healthy tissues against glass could drive consistent and reproducible recovery of compression-induced cartilage deformation, through the mechanism of 'tribological rehydration'. In contrast, the presence of physical cartilage damage, mimicking those injuries known to precipitate PTOA, could compromise tribological rehydration and the sliding-driven recovery of cartilage function. Full-thickness cartilage injuries (i.e. fissures and chondral defects) markedly suppressed sliding-driven tribological rehydration. In contrast, impaction to cartilage, which caused surface associated damage, had little effect on the immediate tribomechanical response of explants to sliding (deformation/strain, tribological rehydration, and friction/lubricity). By leveraging the unique ability of the cSCA configuration to support tribological rehydration, this study permitted the first direct *ex vivo* investigation of injury-dependent strain and friction outcomes in cartilage under testing conditions that replicate and maintain physiologically-relevant levels of fluid load support and frictional outcomes under high sliding speeds (80 mm/s) and moderate compressive stresses (~0.3 MPa). Understanding how injury alters cartilage tribomechanics during sliding sheds light on mechanisms by which cartilage's long-term resilience and low frictional properties are maintained, and can guide studies investigating the functional consequences of physical injury and joint articulation on cartilage health, disease, and rehabilitation.

1. Introduction

Intact articular cartilage is crucial to joint health and function: providing the load bearing and low friction surfaces necessary for joint articulation. Healthy articular cartilage is particularly resilient, retaining exceptional mechanical functionality over millions of reciprocation cycles year in and year out (Eckstein et al., 1999). Notwithstanding this resiliency, cartilage is prone to degeneration, wear, and dysfunction, leading to osteoarthritis (OA). Despite OA being understood as a disease of 'old age', younger individuals that suffer acute and traumatic joint injuries are at significantly increased risk of developing an accelerated form of OA, termed post-traumatic OA (PTOA) (Lieberthal et al., 2015; Buckwalter et al., 2013). Joint injuries can compromise the biomechanical functionality of articular cartilage, i.e. its fluid load support and permeability (Mansour, 2003; Dabiri and Li, 2015; Pawaskar et al., 2007), friction coefficient (Bonnevie et al., 2017; Burris and Moore, 2017), and wear resistance (McCutchen, 1962), through changes to the physical structure of cartilage, including surface roughening or fibrillation (Mow et al., 2005), linear partial and full-thickness fissures (Ewers et al., 2001), and chondral defects (Falah et al., 2010). Understanding how acute articular cartilage injuries influence such tissue-level biomechanics and tribology will help elucidate mechanisms regulating cartilage's long-term resilience and low friction properties, and uncover underlying mechanobiological contributors to PTOA initiation/progression, which can be used to inform improved rehabilitation, prevention, and treatment strategies.

A number of models have been developed to explore the influence of acute joint injuries on articular cartilage health and functionality (Lieberthal et al., 2015; Ewers et al., 2001; Bonnevie et al., 2015; Jeffrey et al., 1995; Moore and Burris, 2015; Torzilli et al., 1999;

* Corresponding author. 161 Colburn Lab, University of Delaware, Newark, DE, 19716, USA.
E-mail addresses: mfarnham@udel.edu (M.S. Farnham), larsonr@udel.edu (R.E. Larson), dlburris@udel.edu (D.L. Burris), cprice@udel.edu (C. Price).

https://doi.org/10.1016/j.jmbbm.2019.103422
Received 28 August 2018; Received in revised form 5 September 2019; Accepted 6 September 2019
Available online 07 September 2019
1751-6161/

Abbreviations

cSCA	convergent stationary contact area explant testing configuration
EoS	end-of-sliding (last cycle of 'active' phase of characterization test)
h	cartilage thickness
k_{Act}	characteristic deformation rate during active sliding period
k_{Sed}	characteristic deformation rate during sedentary compression period
LME	linear mixed effects model
OA	osteoarthritis
PBS	phosphate buffered saline (+protease inhibitors)
PTOA	post-traumatic osteoarthritis
SCA	stationary contact area explant testing configuration
SD-RM	Steel-Dwass repeated measures multiple comparison statistical test (non-parametric)
SoS	start-of-sliding (initial cycle of 'active' phase of characterization test
WSR-PM	Wilcoxon signed rank paired measures statistical test (non-parametric)
δ	deformation
ε	strain
μ_k	kinetic coefficient of friction
τ_{Act}	characteristic time constant during active sliding period
τ_{Sed}	characteristic time constant during sedentary compression period
Ø	diameter

Whittaker et al., 2015; Punzi et al., 2016; Henao-Murillo et al., 2018; Trevino et al., 2017). *In vivo* models have provided crucial information regarding the long-term structural and biological consequences of traumatic injury on joint health and function (Abusara et al., 2011; Milentijevic et al., 2005); however, they often suffer from limited control over loading and movement patterns, and lack precision regarding strain, stress, and frictional assessments. As a result, researchers have turned to *ex vivo* studies, which enable far greater experimental control and resolution, to study the immediate effects of injuries on cartilage biomechanics (Ewers et al., 2001; Henao-Murillo et al., 2018; Argatov and Mishuris, 2015; Bonnevie et al., 2018; Chen et al., 2001; Farquhar et al., 1996; Patwari et al., 2001). *Ex vivo* studies suggest that acute cartilage impact injury does indeed drive detrimental biomechanical outcomes (Bonnevie et al., 2017), but traditional *ex vivo* studies are not without limitations. For example, studies utilizing unconfined compression testing have elucidated the negative consequences of degeneration, injury, and OA on cartilage's compressive biomechanics (Kleeman et al., 2005; Robinson et al., 2016), but the interpretation of such studies is limited to the response of cartilage to static (Gannon et al., 2015) and/or dynamic compression (Gannon et al., 2015; Evans and Quinn, 2006). Unfortunately, such loading doesn't replicate the totality of motions/forces that cartilage endures during articulation (e.g. sliding, migration, rolling, etc.). Instead, testing schemes that include articulation, specifically physiologically-consistent contact geometries and sliding motions, are necessary for studying the biomechanical and tribomechanical response of cartilage to injury, i.e. its deformation/strain, rehydration, and friction/lubrication responses.

A limited number of explant studies that include articulation (i.e. sliding) have begun to highlight how cartilage injuries (e.g. focal defects (Venalainen et al., 2016), injurious impactions (Bonnevie et al., 2017), and early osteoarthritic changes (Desrochers et al., 2013) alter tissue tribomechanics. Chondral defects can cause ~3-fold increases in cartilage stress and strain gradients, leading to abnormal cell death and collagen crosslink failure (Venalainen et al., 2016); while impaction and early osteoarthritic changes have been shown to influence cartilage friction (Bonnevie et al., 2017; Jeffrey et al., 1995; Torzilli et al., 1999; Chen et al., 2001). However, it must be noted that these findings have been established using the 'classical' stationary contact area (SCA) explant testing configuration. In the SCA configuration, small diameter (≤Ø6mm) osteochondral explants are pressed flat against a sliding counterface (e.g. flat-on-glass configuration) and then slid. This configuration allows for the measurement of tissue deformation and friction in response to precisely applied compressive stresses during a variety of *ex vivo* sliding experiments. However, the behavior of cartilage to compression and sliding in classical SCA explant studies differs markedly from that of cartilage *in vivo*. Specifically, in SCA studies, cartilage is unable to sustain physiological-consistent levels of fluid support over time, causing continuously increasing strain and rapid transitions towards supra-physiological friction values. Consequently, care must be exercised in interpreting the results obtained from SCA-based tests within the context of *in vivo* articular cartilage function (Pawaskar et al., 2007; Rajan et al., 2010; Ateshian, 2009; Huang et al., 2005).

Recently, we have 're-discovered' a cartilage explant testing configuration, called the convergent stationary contact area (cSCA), that is unique in its ability to permit the long-term *ex vivo* study of cartilage tribomechanics under more physiologically-consistent sliding conditions and outcomes (Moore and Burris, 2017; Burris and Moore, 2017; Graham et al., 2017a; Graham et al., 2018; Burris et al., 2019). These include the application of sliding speeds (~80 mm/s) and compressive stresses (~0.3 MPa) that are consistent with those observed during gait (Moore and Burris, 2015; Graham et al., 2017b), while simultaneously being able to minimize compressive strains (4–20%) (Brand, 2005), promote high fluid load support (80–95%) (Burris and Moore, 2017; Moore and Burris, 2015; Graham et al., 2017a), and facilitate extremely low friction coefficients ($\mu_K < 0.02$) (Moore and Burris, 2017)- long-term *ex vivo* in the absence of boundary/viscous lubricants (i.e. with only PBS present); outcomes that are unprecedented among studies utilizing SCA configurations. cSCA tests are similar to SCA tests in that osteochondral explants are compressed and slid against a rigid and impermeable counterface while deformation and friction are recorded. However, cSCA explants are unique in that they have larger, convex cartilage surfaces then traditional SCA explants; where the diameter of the cSCA cartilage explant (Ø19mm) is larger than that of the patch of cartilage contacting the counterface (Ø5–6mm). This geometry results in development of wedge-shaped convergence zones at the leading edges of contact (Graham et al., 2017a), which we have proposed support hydrodynamic pressurization of fluid in the converging wedge between the cartilage surface and the counterface during sliding. We theorize that the resultant pressurization of the bathing fluid in the cSCA drives water back into the porous cartilage surface, promoting a sliding-driven reversal and recovery of tissue deformation (on the order of tens to hundreds of microns (Graham et al., 2017a; Moore and Burris, 2017). The observed milliscopic recovery of cartilage deformation could only be explained by a sliding-driven recovery of tissue volume, and thus interstitial fluid (or water content), a process we have termed 'tribological rehydration' (Graham et al., 2017a; Moore and Burris, 2017). This process of competitive rehydration in the cSCA mimics the deformation and interstitial fluid recovery seen during *in vivo* articulation (Eckstein et al., 1999), and by promoting the recovery and preservation of interstitial lubrication, allows for the long-term maintenance of physiologically-consistent kinetic friction coefficient values ($\mu_\kappa \approx 0.02$) (Burris and Moore, 2017; Graham et al., 2017a; Moore and Burris, 2017), even in the absence of boundary/viscous lubricants (Graham et al., 2017a; Moore and Burris, 2017). Our discovery of

tribological rehydration has allowed us to use the cSCA to explore a variety of aspects of cartilage's tribomechanical behavior under 'physiologically consistent' and 'fully sustainable' conditions of high sliding speeds, high compressive stresses, high interstitial fluid pressures, low tissue strains, and low friction coefficients (Burris and Moore, 2017; Graham et al., 2017a); conditions that are either not achievable or are difficult to control for in classical SCA (Bonnevie et al., 2017; Venalainen et al., 2016; Desrochers et al., 2013) or migrating stationary contact area (MCA) (Bonnevie et al., 2014) testing configurations. Thus, the goal of this study was to use the novel cSCA configuration to determine how clinically relevant mechanical injuries (impacts, fissures, defects) influence and/or compromise sliding-induced tribological rehydration and hydration-dependent cartilage biomechanical functionality under conditions of physiologically-consistent loading and sliding.

2. Methods

2.1. Tissue specimens

All specimens were obtained from mature bovine stifle joints of cattle slaughtered at a local abattoir (Bowman's Butcher Shop, Churchville, MD) and intact joints were transferred, frozen, to the research lab (a total of 12 joints were collected by the abattoir from ~1.5–3.5 y.o. steer). Joints were thawed at 4 °C over the course of 48-h, then Ø19mm osteochondral cores were removed from the centerline of each femoral condyle (Fig. 1A) with a coring bit and drill (Graham et al., 2017a); 6–8 cores were obtained from each joint. Cores were then rinsed with 1x phosphate buffered saline (PBS), the underlying bone was trimmed to approximately 15 mm in height using an ISOMET low-speed saw (Buehler, Lake Bluff, IL), and the *in vivo* sliding orientation, taken to be the principle direction of sliding between the condyle and tibial plateau, was indicated on each explant. After extraction and in between tests, cores were stored in PBS + protease inhibitors (5 mM EDTA + 5 mM benzamidine hydrochloride hydrate, Sigma-Aldrich, St. Louis, MO; herein referred to as PBS) at 4 °C.

2.2. In situ tribometer

A custom-built reciprocating materials testing device (*in situ* tribometer), described previously (Moore and Burris, 2017), was used in this study (Fig. 1B). Briefly, this device holds a cartilage explant atop a 3-axis load cell that measures normal and frictional forces, while cartilage deformation is measured via a linear variable differential transformer. The tribometer enables compression of the explant against an impermeable glass slide, and is capable of applying forces of 0–7.5N across the contact while the glass slide can be slid back and forth across the sample at speeds ranging from 0 – 80 mm/s over a track length of ± 20 mm. Deformation (δ), normal force (F_N), friction force (F_F), and kinetic friction coefficient (μ_k) are recorded during each test using a custom LabVIEW program (National Instruments, Austin, TX) (Graham et al., 2017a, 2018; Moore and Burris, 2017). Briefly, cartilage deformation, normal force, and friction force are measured continuously, at 500HZ, throughout each reciprocal cycle. Within each cycle, deformation, normal force, friction force, and kinetic friction coefficient ($\mu_k = F_F/F_N$) values are automatically extracted from the data stream at the middle portion of each sliding phase, during steady-state sliding. For each cycle of sliding, the respective steady-state sliding data derived from the positive- and negative-sliding directions are averaged to provide a single-cycle data point that is recorded.

2.3. Testing protocols

2.3.1. Diagnostic tests

Prior to testing, each explant was inspected for surface damage using India Ink under a stereomicroscope (Zeiss Stemi 2000-CS, Oberkochen, Germany); India Ink diluted in water (1:1 ratio) was placed upon the surface of the cartilage using a dropper (1–2 drops), and excess India Ink was removed with a PBS-moistened wipe. Pristine cartilage appeared a uniform white following India Ink removal, while cartilage with preexisting cracks/fissures on the surface collected ink visible to the naked eye and under the stereomicroscope (examples shown, Fig. 2). Explants with visible surface damage were excluded from the study. Remaining samples then underwent a diagnostic loading and sliding test to ensure that each sample included in the study exhibited tribological rehydration at baseline. These diagnostic tests began with 7N of static compression for 10 min, followed by reciprocal sliding at 80 mm/s against the glass counterface for 2 min while compression was maintained. The applied 7N load resulted in an initial compressive stress of ~0.3 MPa, which approximates the lower range of spatially averaged contact stresses observed during standing (Brand, 2005), and the sliding speed of 80 mm/s is similar to the tangential cartilage speeds induced by knee joint articulation during walking (Moore and Burris, 2017; Graham et al., 2017b). In order to be included in the study, samples had to meet two diagnostic criteria: i) minimum kinetic friction coefficients $\mu_\kappa \leq 0.1$; and ii) observation of sliding-induced tribological rehydration during the short diagnostic test, which was defined as either sliding-induced recovery of compression-driven cartilage deformation during high-speed sliding, or the sliding-driven halting and prevention of further compression-induced deformation. Following reciprocation, the applied load was removed, and the samples were allowed to free-swell for a minimum of 2 h before further testing was conducted.

2.3.2. Tribological rehydration characterization protocol

Each sample underwent a 1-h tribological rehydration characterization protocol (Fig. 1C), starting with 30 min of static compression at an initial load of 7N, which we term the 'sedentary' period, followed by 30 min of reciprocal sliding at 80 mm/s while this compressive load was maintained, the 'active' period. The 30-min sedentary period is sufficient to drive fluid exudation from the cartilage samples and establish

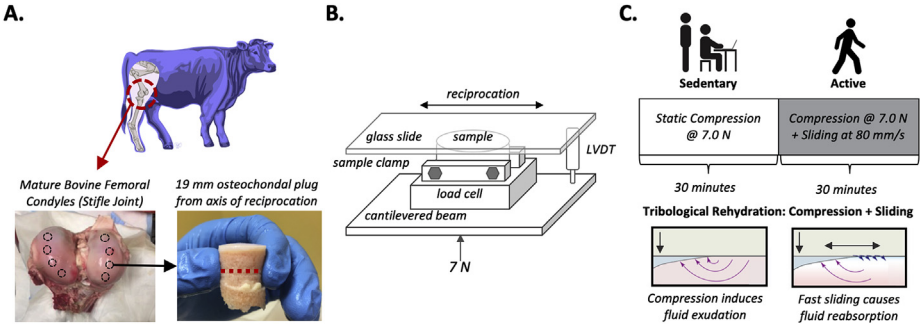

Fig. 1. A) Schematic illustrating the locations from which osteochondral explants were removed from the femoral condyles of bovine stifle joints. B) Schematic of the cSCA explant testing configuration within the *in situ* materials tester (a.k.a. *in situ* tribometer) and the device's data collection hardware. C) Sedentary behaviors were mimicked in the *in situ* tribology setup by statically compressing cartilage explants at 7N, and active behaviors (i.e. walking) were mimicked by sliding cartilage at 80 mm/s in this compressed state. The abbreviated tribological rehydration protocol started with 30 min of sedentary static compression driving fluid exudation, followed by 30 min of active sliding, causing sliding-induced fluid reabsorption, i.e. tribological rehydration.

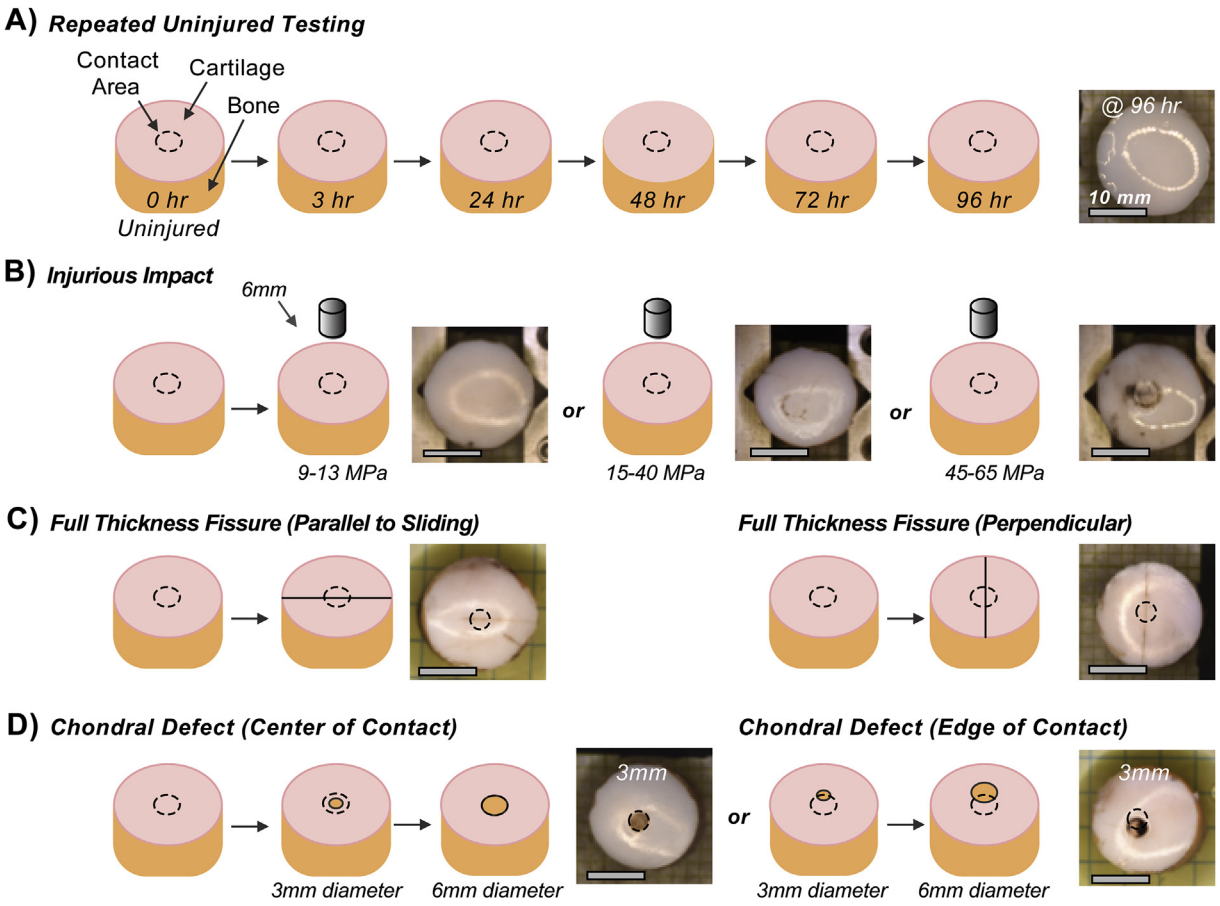

Fig. 2. Starting with each explant in the uninjured state, tribological rehydration characterizations were performed A) on uninjured explants twice on the day of extraction and once on each of the following 4 days to address the repeatability of tribological rehydration and biomechanical assessment between tests and over time; B) on explants impacted with a 6 mm indenter applying peak impact stresses of 9–13, 15–40, or 45–65 MPa (see Supplemental Appendix B; Fig. B1); C) on explants with full-thickness cartilage fissures imparted by a scalpel, either parallel (left) or perpendicular (right) to the direction of sliding; and D) on explants that had chondral defects of 3 mm and then 6 mm in diameter generated in either the center (left) or edge (right) of cSCA contact. Contact area is denoted on images in C and D to clarify how injury was oriented with regards to actual contact area.

the response of the samples to compression alone. During the 30-min active period, sliding at 80 mm/s drives fluid back into the cSCA cartilage explant as a result of tribological rehydration (Burris and Moore, 2017), allowing quantification of cartilage deformation/strain recovery and subsequent friction reduction in the cSCA due to high-speed sliding. Following this initial characterization, individual samples were then allowed to passively free-swell in PBS for at least 2 h, allowing recovery to their initial swollen state before continuing on into study arms for A) assessment of the short- and long-term repeatability of tribological rehydration, or the influence of B) injurious impaction, C) cartilage fissures, or D) chondral defects on tribological rehydration (described in Fig. 2).

2.3.3. Repeatability of tribological rehydration and biomechanical assessment

To assess the repeatability of our assessment protocols (Fig. 2A), tribological rehydration characterization was repeated twice on day 1 (the day of sample extraction from the joint), allowing at least 2 h for free-swelling in PBS between tests, to test for short-term inter-test repeatability, and then daily on days 2–5 to test for longitudinal repeatability (n = 8 samples). After the final test on day 5, explants were stained with India ink to assess surface damage following the repeated tests.

2.3.4. Influence of injurious impact on tribological rehydration

A custom designed drop tower impactor (Fig. B1; Supplemental Appendix B) was used to deliver controlled injurious impacts to osteochondral plugs (Jeffrey et al., 1995; Torzilli et al., 1999; Chen et al., 2001). Each explant (N = 6 per group) was first tested in the uninjured state using the tribological rehydration characterization protocol (Section 2.3.2), allowed to reswell in PBS, impacted, and then tribological characterized again in the injured state (Fig. 2B). For each sample, the cSCA region of contact was identified as the region of cartilage that initially contacted and flattened against the glass counterface during the uninjured sliding test; this location was noted and the subsequent injurious impact was delivered to the center of this cSCA contact region (for bovine femoral condyle explants these contact areas are typically ~∅6 mm). Following characterization in the uninjured state, one of three different magnitude impacts were delivered with a ∅6 mm impactor tip from calibrated drop heights; these impacts were classified as either low (9–13 MPa peak stress), moderate (15–40 MPa peak stress), or severe (45–65 MPa peak stress) in magnitude based on previous studies (actual range of recorded impact stresses in each grouping are indicated) (Jeffrey et al., 1995; Torzilli et al., 1999; Chen et al., 2001). On average, impact duration ranged from 1.3 – 4.6 ms, resulting in impact stress rates of 2700–43,450 MPa/s, and impact impulses of 27–107 N·s. India ink staining and stereomicroscopy visualization were again used following impact to qualitatively assess for the presence of impact-induced surface disruptions.

2.3.5. Influence of full-thickness cartilage fissures on tribological rehydration

Two types of full-thickness fissures were investigated: fissures parallel and perpendicular to the *in vivo* sliding direction (N = 6 for each fissure direction, Fig. 2C). Each explant was first tested in the uninjured state using our tribological rehydration characterization protocol (Section 2.3.2), and the cSCA contact region was noted to enable the creation of a subsequent fissure through the center of the contact region. Following initial characterization in the uninjured state, a fissure was made via a scalpel blade cut through the full thickness of the cartilage down to the underlying bone and across the width of the plug. Explants free-swelled in PBS for 2 h between tests.

2.3.6. Influence of chondral defects on tribological rehydration

Two types of chondral defects were investigated: defects in the center of each cSCA contact patch and defects at the edge of contact (Fig. 2D). Each explant (N = 6) was first tested in the uninjured state using the tribological rehydration characterization protocol (Section 2.3.2), and the cSCA region of contact was noted to enable creation of defects in the center/edge of the contact region. Following initial testing, a ∅3 mm defect was made, and explants underwent tribological characterization a second time before a ∅6 mm defect surrounding the original defect was created and the explants were tested a third time. Chondral defects were made using biopsy punches: the cartilage layer was first punched down to the bone and then removed using a scalpel blade. Explants free-swelled in PBS for 2 h between tests.

2.4. Data analysis

Once samples were subject to their full complement of characterizations, they were bisected through the center of the cSCA contact (or immediately adjacent to the site of injury), imaged using a stereomicroscope, and the cartilage thickness was measured by tracing the articular cartilage across the entire width of the bisected explant in MATLAB and obtaining an average thickness using a Euclidean distance transform. Measures of tissue biomechanics, including deformation (δ) and kinetic friction coefficient (μ_k) were extracted from the raw data for the first reciprocal sliding cycle (start-of-sliding [SoS] phase), the last sliding (end-of-sliding [EoS] phase), and as averaged over each characterization protocol (Fig. 3A and B) (Graham et al., 2018). Measures of strain (ε) were defined based on optically measured cartilage thickness (h) (Eq. 1).

$$\text{Strain} = \varepsilon = \frac{\delta}{h} \quad (1)$$

During both the 'sedentary' (0–30min) and 'active' periods (30–60min), the shape of the static load-induced strain and sliding-induced strain recovery curves approximated those of one-phase exponential association and decay, respectively (Fig. 3A, Eqs. A1 & 2). Accordingly, the characteristic time constants (τ_{Sed} and τ_{Act}) of these curves could be utilized to approximate the temporal dynamics of static load-induced deformation and sliding-induced tribological rehydration, respectively. The methodology utilized to extract these characteristic time constants from the raw data is described fully in Appendix A: Supplemental Methods. Briefly, to minimize curve fitting complexity (Eqs. A3 & 4), time-dependent deformation data were first normalized to their respective start-of-sedentary and start-of-sliding strain values (Fig. 3C, Eq. A5), then the natural log of these normalized curves was plotted against time (Fig. 3D). Over the initial 3–4 min of each period, this treatment generated quasi-linear curves; the slopes of which provided measures of initial static load-induced and sliding-induced deformation rates, k_{Sed} and k_{Act}, respectively (Eqs. A6 & 7), from which the characteristic time constants ($\tau_{Sed} = 1/k_{Sed}$ and $\tau_{Act} = 1/k_{Act}$) could be estimated. In this manner, negative k-values, and thus $\tau < 0$, indicate net recovery of compressive deformation (i.e. tribological rehydration); positive k-values, and thus $\tau > 0$, indicate pure compression-induced deformation (during the sedentary period) or continued deformation due to compromised tribological rehydration (during the sliding period); and k-values ≈ 0 denote the condition where no additional net deformation was observed during sliding, and that compression-induced deformation and sliding-induced tribological rehydration were in balance. As such, samples with k-values ≈ 0 were not assigned τ-values, but instead separated from the other data for clarity (see Figs. 7 and 8, panel D).

All data was processed and analyzed using MATLAB (MathWorks, Natick, MA) and the JMP statistical software package (SAS Institute, Cary, NC). Data outliers were identified using a mean absolute deviation outliers test for strain recovery and end-of-sliding friction coefficient; data was recollected with new samples to ensure each group had

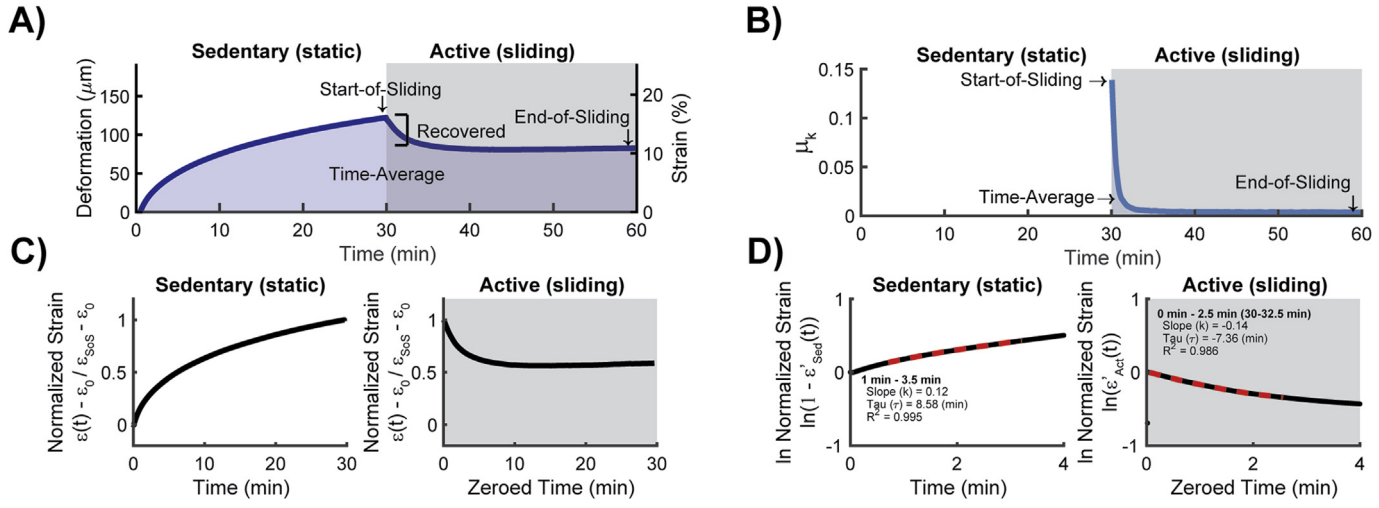

Fig. 3. A) Representative deformation and strain traces, and B) kinetic coefficient of friction data traces illustrating the biomechanical parameters of interest. The first 30 min of data (white background) indicate the response of the cartilage to sedentary compression (7N). The last 30 min of data (grey background) indicate the response of the cartilage to reciprocal sliding (at 80 mm/s) while under compression (7N). The blue shaded areas under each curve indicate the data used to calculate time-average deformation and friction responses. C) Data were normalized using Eq. A5 for sedentary and active sliding, D) which was then used to calculate deformation time constants (Eqs. A6 & 7; black = normalized data, dashed red lines = curve fits). For the sedentary period the deformation rate of the linear region immediately past the short toe-region (time = 1–3.5min) was used. For the active period, time was normalized to start at zero (instead of 30 min) and the deformation rate was calculated over t = 0–2.5min, as no toe region was observed.

N = 6–8 included samples/data after outlier removal, only non-outlier data are presented for clarity (repeatability: 0 outliers were removed from 8 samples, impact: 3 outliers out of 21, fissures: 4 outliers out of 18, defects: 6 outliers out of 12). For the repeatability portion of the study (Section 2.3.3), linear mixed effects (LME) modeling was used to determine if tribological rehydration and biomechanical assessments varied significantly between subsequently repeated characterization tests (or equivalently, over time) across the 5-day testing period. LMEs are extensions of generalized linear model analyses that allow for the determination and separation of contributions from both fixed (i.e. test number, or time) and random (i.e. sample identity) effects on our tribomechanical outcomes. To determine potential variability between repeated tests on the same day, the first two time points (0 and 3 h) were investigated in more detail, using non-parametric Wilcoxon signed rank paired-measures (WSR-PM) tests comparing the median of the change between hour 3 and hour 0. To identify if statistically significant differences existed among biomechanical parameters before and after injury, non-parametric WSR-PM tests were performed for the impact injury (Section 2.3.4) and the fissure injuries (Section 2.3.5), and Steel-Dwass repeated-measures (SD-RM) multiple comparison tests used for the chondral defect injuries (Section 2.3.6), as one-sample Kolmogorov-Smirnov tests indicated the data was not normally distributed (JMP, SAS Institute, Cary, NC). Statistical significance was set at $p < 0.05$ for all statistical tests. Actual power for each injury type was calculated after data collection was complete (G*Power, denoted in results figure captions).

3. Results

3.1. Repeatability of tribological rehydration

Using our *in situ* tribology setup, the strain and kinetic friction responses of individual cartilage cSCA explants were both consistent and repeatable from test-to-test, and thus day-to-day, over five days of repeated testing (Figs. 3 and 4). Additionally, staining with India ink before and after testing showed qualitatively similar cartilage surfaces, indicating that repeated testing in the cSCA did not incur visible damage or wear. In general, load-induced deformation under 'sedentary' (static) compression and deformation recovery during 'active' loaded sliding were consistent across all tests; the explant with the median strain recovery response is shown in Fig. 4. Kinetic friction behavior was also consistent among the repeated sliding tests; following 30-min of static compression, each test started with an initial spike in the kinetic friction coefficient during the first reciprocal sliding cycle (μ_k = 0.17–0.20), and as sliding-induced tribological rehydration occurred (defined as sliding-driven strain recovery) kinetic friction values rapidly dropped to markedly-low equilibrium (end-of-sliding) values (μ_k = 0.03–0.06). It is noted that the tribological outcomes observed in this investigation aligned with those from prior cSCA studies (Graham et al., 2017a; Moore and Burris, 2017), again demonstrating the unique ability of high-speed sliding to promote the recovery and long-term maintenance of high interstitial fluid pressures, low cartilage strains, and low friction coefficients in the cSCA under high-speed sliding and absent boundary/viscous lubricants.

Despite the presence of statistically significant inter-sample variability in all static compressive and sliding-induced tribomechanical outcomes (different intercepts; $p < 0.001$; Fig. 5), LME model analysis illustrated that for any given sample, sliding-driven tribological rehydration (i.e. strain recovery) remained consistent across all of the repeated characterization tests (groupwise slopes no different from zero [0]). We observed no statistically significant influence of test number, and thus time, on sliding-induced strain recovery ($p = 0.64$; Fig. 5A), the temporal dynamics of start-of-sedentary or start-of-sliding deformation (i.e. deformation time constants; $p = 0.71, 0.21$; Fig. 5B and C, respectively), start-of-sliding strain ($p = 0.38$; Fig. 5D), end-of-sliding strain ($p = 0.32$; Fig. 5E), or time-averaged strain ($p = 0.26$; Fig. 5F). The only tribomechanical metric that exhibited a test-dependent change was kinetic friction at the start-of-sliding ($p = 0.03$; Fig. 5G), where a statically significant increase in start-of-sliding kinetic friction was observed between the first and second repeated characterization tests on day one (comparison of 0- to 3-h tests, $p = 0.02$; Fig. B2G, Supplemental Appendix B). Friction parameters dependent upon tribological rehydration, i.e. end-of-sliding kinetic friction and time-averaged kinetic friction, did not vary among the repeated

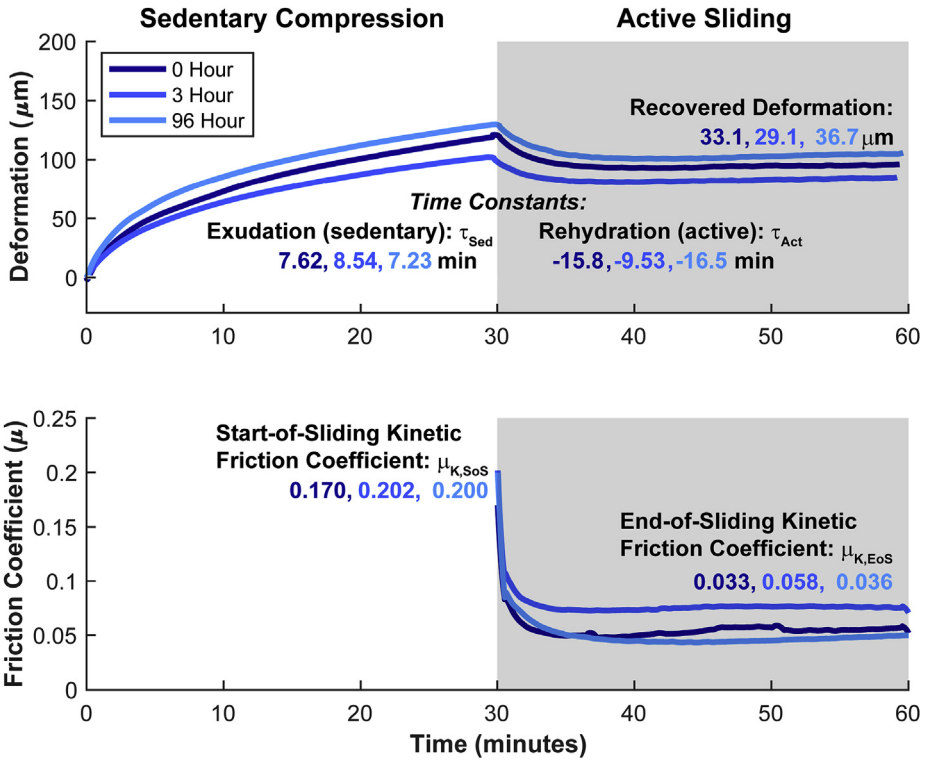

Fig. 4. Deformation (top) and kinetic friction (bottom) responses from repeated tribological characterization tests on a representative osteochondral explant indicating similar deformation and friction behaviors across all five days of testing. Recovered deformation, and kinetic friction coefficient values during the first (start-of-sliding) and last (end-of-sliding) sliding cycles are indicated. Additionally, deformation time constants during 7N compression ('sedentary'; τ_{Sed}, white background) and 80 mm/s reciprocal sliding ('active'; τ_{Act}, grey background) were determined (see Fig. 3, Eqs. A1-7 Supplemental Appendix A).

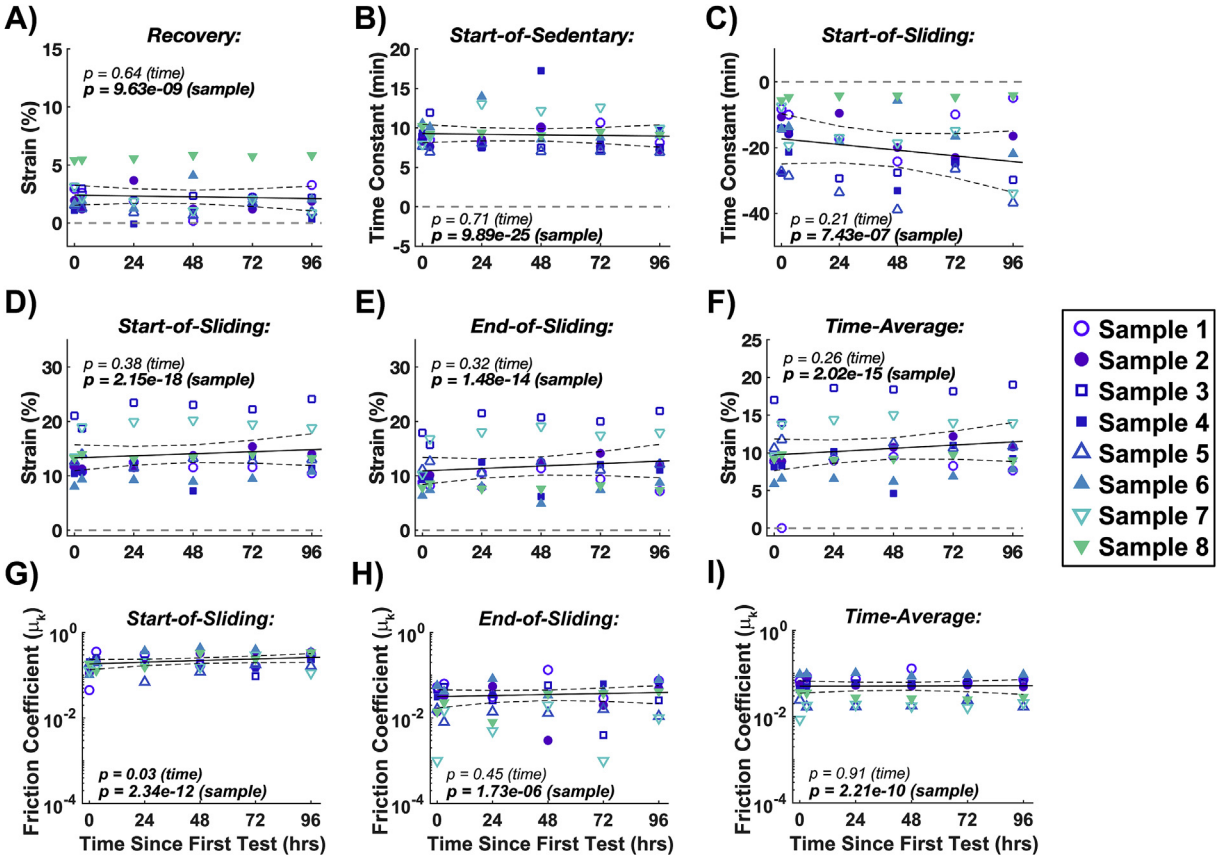

Fig. 5. Assessment of the consistency and repeatability of tribomechanical outcomes in the cSCA across multiple characterizations over four days of testing. Group-wise A) strain recovery, B) start-of-sedentary deformation time constant (1–3.5min), C) start-of-sliding deformation time constant (30–32.5min), D) start-of-sliding strain, E) end-of-sliding strain, and F) time-average strain outcomes remained consistent and unchanged over the entirety of the 5-day study. Although G) kinetic friction in the first, start-of-sliding cycle increased significantly over the 5-day testing period (p = 0.03), H) end-of-sliding kinetic friction, and I) time-averaged kinetic friction remained consistent and unchanged. The relationship between each individual biomechanical outcome and time following the initial biomechanical characterization is indicated by solid lines (average linear trends; a.k.a. slopes) and dashed lines (95% confidence intervals for these trends), as determined by LME analysis. Each individual explant is denoted by a different shape/color symbol to highlight individual trends over the repeated tests.

tribological rehydration characterizations (p = 0.45, 0.91; Fig. 5H and I, respectively).

3.2. Influence of injurious impact on tribological rehydration

We did not observe statistically significant changes in the tribomechanical responses of cSCA cartilage explants to high-speed reciprocal sliding after impact with a Ø6mm indenter. Paired pre- and post-impact strain responses showed maintenance of tribological rehydration (i.e. strain recovery) for plugs in the mild, moderate, and severe impact groups (sample traces shown in Fig. 6A represent those with the median strain recovery response in each group; curves illustrating the least affected, median, and most affected responses in each impact group can be found in the Supplemental Appendix, Fig. B3). The initial biomechanical responses of uninjured cartilage to static loading and sliding were similar among the impact testing groups (p = 0.078–0.47, SD-MC, Fig. 6D-L), and consistent with those found in the repeatability portion of this study. Relative to each sample's paired uninjured characterization test, none of the impact severities tested caused statistically significant changes in strain recovery (i.e. tribological rehydration magnitude or temporal dynamics, p = 0.230–0.810, 0.230–0.521, WSR-PM; Fig. 6D, F, respectively) or any other strain or kinetic friction outcomes except for the sedentary phase deformation time constant (τ_{Sed}), which decreased following the delivery of a severe impact (p = 0.008; Fig. 6C).

3.3. Influence of cartilage fissures on tribological rehydration

Despite again observing statistically significant inter-sample variability in tribomechanical outcomes amongst cSCA explants before the generation of full thickness cartilage fissures (p = 0.012–0.812, WSR-PM), we identified clear evidence that full thickness fissure injuries compromised sliding-driven tribological rehydration (i.e. strain recovery) in the cSCA (Fig. 7A). In the presence of a single full-thickness fissure through the cSCA contact patch, either in a direction parallel to or perpendicular to sliding, strain recovery during sliding significantly decreased compared to each explant's respective uninjured characterization (p = 0.005 for both, WSR-PM; Fig. 7B). All samples experienced a reduction in sliding-induced strain recovery in the presence of a fissure injury, and continued load-induced deformation (i.e. net loss of tribological rehydration) was observed in two out of six parallel fissure explants and three out of six perpendicular fissure explants.

On average, full-thickness fissures had inconsistent to minimal influence on the dynamics of static load-induced compression (start-of-sedentary deformation time constant τ_{Sed}; Fig. 7C). However, the presence of a full-thickness fissure paralleling the direction of sliding did drive significantly slower deformation time constants during sliding (p = 0.031, WSR-PM; Fig. 7D, all samples exhibited a reduction in τ_{Act}), again confirming that this injury could compromise sliding-driven tribological rehydration in cSCA explants. At a more granular-level, fissures parallel to sliding led to statistically significantly increases in start-of-sliding (p = 0.031; Fig. 7E), end-of-sliding (p = 0.008; Fig. 7F), and time-averaged strain (p = 0.020; Fig. 7G), and time-averaged

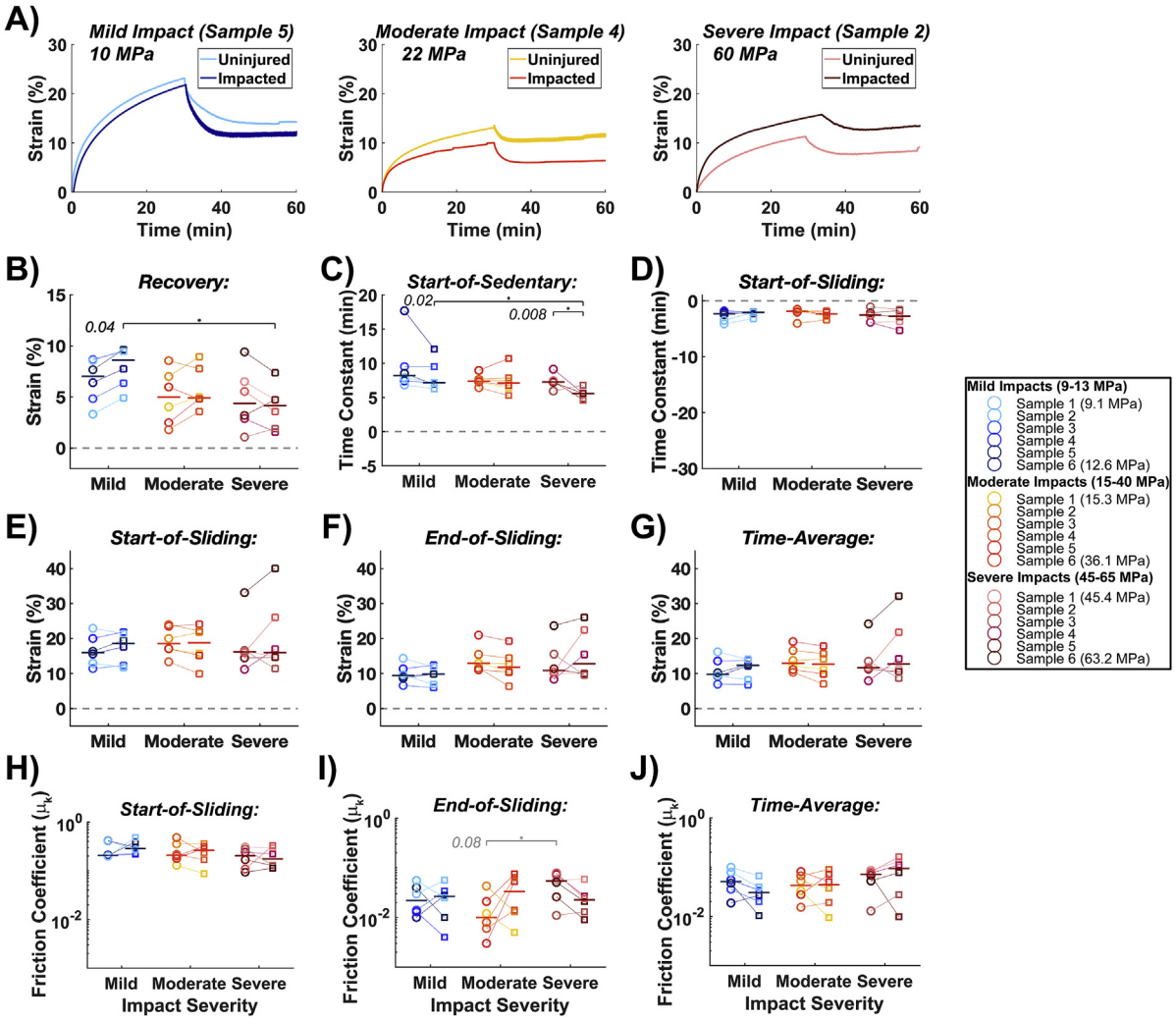

Fig. 6. cSCA Tribomechanical outcomes following injurious impact. A) Representative 'sedentary' and 'active' deformation curves from before and after mild (leftmost data on graph), moderate (middle data), or severe impact (rightmost data on graph) to cSCA samples. The sample exhibiting the median strain recovery response in each impact dataset is shown. Quantified tribomechanical outcomes included B) strain recovery, C) start-of-sedentary deformation time constant (1–3.5min), D) start-of-sliding deformation time constant (30–32.5min), E) start-of-sliding strain, F) end-of-sliding strain, G) time-averaged strain, H) start-of-sliding kinetic friction, I) end-of-sliding kinetic friction, and J) time-averaged kinetic friction. Median values are denoted by horizontal bars, with each sample represented by a different color. Statistical significance was determined using nonparametric Wilcoxon signed rank paired-comparison (WSR-PM) and Steel-Dwass multiple comparison (SD MC) tests ($\alpha = 0.05$; $\beta = 0.83$).

kinetic friction ($p = 0.005$; Fig. 7J), compared to their pairwise uninjured tests. For fissures perpendicular to sliding, only time-averaged kinetic friction trended toward an increase between the injured and uninjured state ($p = 0.066$; Fig. 7J).

3.4. Influence of chondral defects on tribological rehydration

In general, chondral defects altered the response of cSCA explants to static compression and compromised sliding-induced tribological rehydration (Fig. 8); as defect size increased, static deformation tended to increase, and sliding-induced strain recovery tended to decrease relative to each explant's uninjured test (Fig. 8B). Indeed, net strain recovery (i.e. tribological rehydration) was completely suppressed in two out of five Ø6mm center defects and four out of six Ø6mm edge defects. In the presence of the largest center of contact defect, the speed of static load-induced compression increased (τ_{Sed} decreased), albeit non-significantly ($p = 0.066$, SW-RM; Fig. 8C), compared to their uninjured tests. Minor increases in τ_{Sed} following edge-of-contact defects and decreases in τ_{Sed} following Ø3mm center defects were not statistically significant. During sliding, the presence of large defects in both the center and at the edge of the cSCA contact led to non-significant decreases in the rate of sliding-induced strain recovery ($p = 0.066$ for both Ø6m defects; Fig. 8D). Comparison of individual strain and kinetic friction outcomes in cSCA explants before and after chondral defect generation illustrated that defects within the center of contact could drive increases in peak strains under static loading (i.e. at the start of sliding; $p = 0.078$ for both Ø3 & Ø6mm; Fig. 8E) and at the end of sliding ($p = 0.078$ for both; Fig. 8F), and increase time-averaged strain ($p = 0.053$ for Ø6mm; Fig. 8G). As the center of contact defects were enlarged from Ø3 to Ø6mm, they drove appreciable increases in start-of-sliding ($p = 0.053$; Fig. 8E), end-of-sliding ($p = 0.228$; Fig. 8I) and time-averaged kinetic friction ($p = 0.078$; Fig. 8J). Compared to their paired uninjured tests, chondral defect injuries at the edge of the cSCA contact patch drove increases in peak strains prior to the start-of-sliding ($p = 0.014$ & 0.035 for Ø3 to Ø6mm defects, respectively; Fig. 8E), at the end of sliding ($p = 0.053$ & 0.035, respectively; Fig. 8F), and as averaged over the entire characterization test ($p = 0.022$ & 0.053, respectively; Fig. 8G). Enlarging these edge-of-contact defects from Ø3 to Ø6mm led to more subtle increases in start-of-sliding, end-of-sliding, and time-averaged friction (Fig. 8H–J).

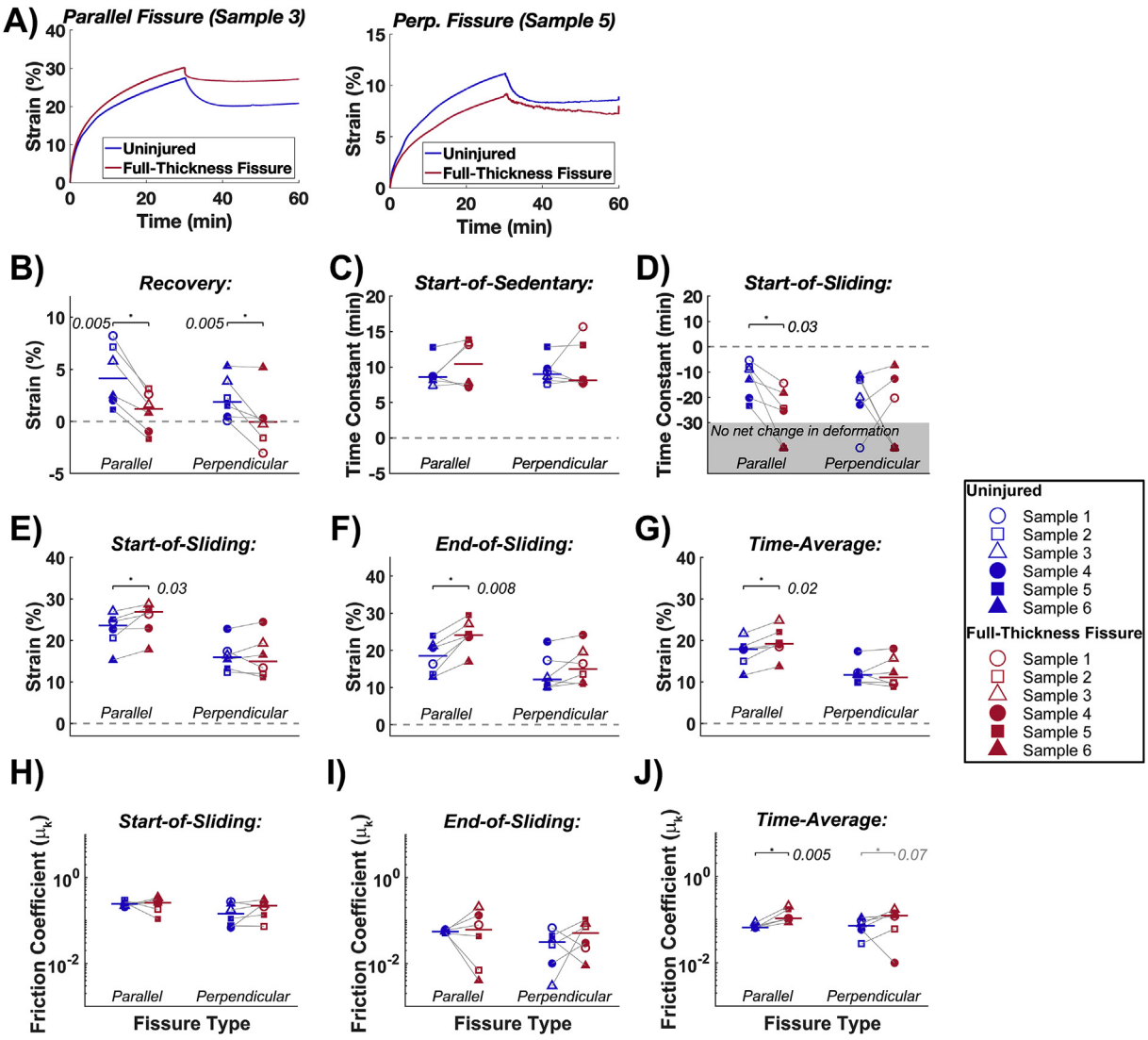

Fig. 7. cSCA Tribomechanical outcomes in the presence of full-thickness cartilage fissures. A) Representative 'sedentary' and 'active' deformation curves before and after generation of full-thickness cartilage fissures. The samples exhibiting the median strain recovery response in each dataset are shown. Tribomechanical responses quantified before (blue) and after (red) injury for parallel (leftmost data on graph) and perpendicular (rightmost data on graph) fissures included B) strain recovery, C) start-of-sedentary deformation time constant (1–3.5min), D) start-of-sliding deformation time constant (30–32.5min), E) start-of-sliding strain, F) end-of-sliding strain, G) time-averaged strain, H) start-of-sliding kinetic friction, I) end-of-sliding kinetic friction, and J) time-averaged kinetic friction. Median values are denoted by horizontal bars, with each sample represented by a different shape. Note that τ_{Act} values less than −30 min were defined as not exhibiting additional net deformation during the active sliding period, and are anchored to the grey shaded region for clarity. Statistical significance was determined using nonparametric Wilcoxon signed rank paired-comparison (WSR-PM) tests ($\alpha = 0.05$; $\beta = 0.94$).

4. Discussion

While known relationships exist between articular cartilage injury and the development of PTOA, how acute injuries drive the rapid progression of osteoarthritic changes remains unknown. Here we leveraged the innovative cSCA cartilage explant testing configuration, and its recently discovered ability to promote sliding-induced tribological rehydration, to demonstrate how clinically-relevant physical injuries to cartilage influence tribological rehydration and tribomechanics under physiologically-consistent sliding and loading conditions (i.e. sliding speeds that approximate those seen during gait, and compressive strains that mimic those of *in vivo* weight-bearing). We showed that cartilage injuries associated with full-thickness damage to the tissue (i.e. linear fissures and chondral defects) could immediately and markedly decrease the ability of articular cartilage to support sliding-induced tribological rehydration in the cSCA, possibly by generating alternative pathways by which pressurized bathing or interstitial fluid can escape the 'sealed' cSCA contact. In contrast, delivery of injurious impacts to the cSCA explants, which caused more surface-limited damage, had remarkably little influence on tribological rehydration (i.e. strain recovery), possibly due to such damage capable of being more-effectively hydrodynamically 'sealed off' from the convergent wedges. Thus, it appears that large, full-thickness damage can immediately compromise cartilage's ability to support tribological rehydration and the biomechanical and tribological properties necessary for its phenomenal resiliency, potentially placing the long-term health of cartilage into immediate jeopardy. Conversely, injuries that are limited to the cartilage surface (i.e. our impacts) may instead precipitate tissue dysfunction through more complex cell-mediated mechanobiological processes, as opposed to primarily mechanically-driven mechanisms.

To establish the consistency of tribological rehydration in cSCA explants over time and the test-to-test reproducibility of our cSCA characterization protocol and outcome assessments, we performed

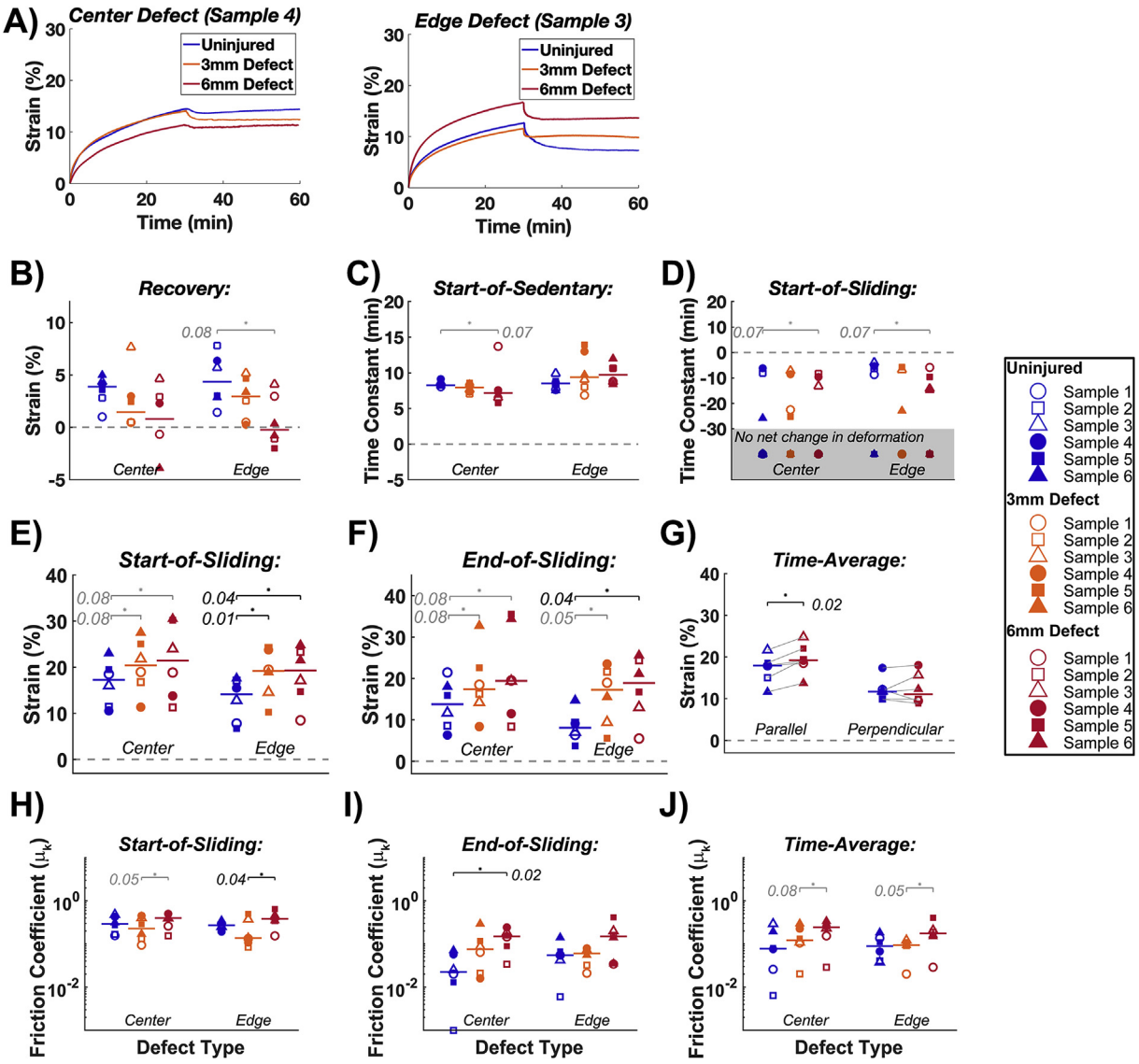

Fig. 8. Tribomechanical outcomes following the generation of chondral defects within cSCA explants. A) Representative deformation curves before and again after the subsequent generation of 3 and 6 mm defects in either the center or edge of the cSCA contact. The sample exhibiting the median strain recovery response in each dataset is shown. Tribomechanical responses quantified before (blue) injury, and after subsequent Ø3mm (orange) and Ø6mm (red) chondral defects were made at either the center (leftmost data in each graph) or edge of contact (rightmost data) included: B) strain recovery, C) start-of-sedentary deformation time constant (1–3.5min), D) start-of-sliding deformation time constant (30–32.5min), E) start-of-sliding strain, F) end-of-sliding strain, G) time-averaged strain, H) start-of-sliding kinetic friction, I) end-of-sliding kinetic friction, and J) time-averaged kinetic friction. Median values are denoted by horizontal bars, with each sample represented by a different shape. Note that τ_{Act} values less than −30 min were defined as having not exhibited additional net deformation during the active sliding period, and are anchored to the grey shaded region for clarity. Statistical significance was determined using nonparametric Steel-Dwass repeated-measures (SD-RM) multiple comparison tests ($\alpha = 0.05$; $\beta = 0.99$).

longitudinal tribological characterizations on individual samples (Section 2.3.3). These repeated-measures/characterizations studies, which accommodated for intrinsic variability among individual samples, indicated that tribological rehydration was consistent in each explant from test-to-test, with no aspect of sliding-induced tribological rehydration being significantly influenced by subsequent testing (Fig. B2; Supplemental Appendix B) or short-term (5 day) storage in PBS (Fig. 5). Only start-of-sliding kinetic friction, which is not intrinsically tied to tribological rehydration, but instead to time-dependent changes in strain and boundary lubrication mechanisms (Kienle et al., 2015), changed over the 5-day testing period (increasing, on average, from 0.139 – 0.259 for the 8 explants tested); with much of this change occurring between the two repeat tests on the initial testing day (Fig. B2G, Supplemental Appendix B). Because we did not observe significant changes in start-of-sliding strain amongst the repeated tests, it is unlikely that this initial increase in start-of-sliding friction was due to test-dependent differences in interstitial hydration and lubrication. It is more likely that these changes were due to sliding-induced removal/shearing off of friction-reducing molecules from the cartilage surface. If such lubricant molecules were 'sloughed-off' during the sliding phase of our first test, this would explain the higher kinetic frictions during the start-up cycles of subsequent characterization tests since our PBS bathing solution was not supplemented with boundary lubricants (Caligaris and Ateshian, 2008). Nonetheless, once sliding started and tribological rehydration was initiated, these initially high kinetic friction values decreased rapidly over the first few reciprocation cycles, promoting very low friction values that were maintained over the remainder of each subsequent sliding period. These results attest to the robust nature of the cSCA testing configuration, its ability to repeatedly drive both stable and physiologically-consistent biomechanical

outcomes (i.e. strain recovery and low friction) through tribological rehydration, and its appropriateness for detecting changes in the biomechanical function of articular cartilage due to acute 'injury' using 'pair-wise' (i.e. repeated measures) experimental testing schemes.

Considering the injuries delivered to the cSCA explants, the most surprising finding came from the injurious impaction tests (Section 2.3.4). Unexpectedly, single acute injurious impacts, even at the highest impact stresses tested (up to 63 MPa), did not markedly compromise the immediate biomechanical and tribological rehydration response of cSCA explants during compression and sliding (Fig. 6). In fact, all impacted samples retained positive strain recovery and negative deformation time constants following injury, (Fig. 6B, D), indicating the presence of meaningful sliding-induced recovery of cartilage thickness, or tribological rehydration, even in the face of impact stresses shown to alter matrix integrity and cartilage homeostasis (Jeffrey et al., 1995; Torzilli et al., 1999; Chen et al., 2001). While this might have been expected for mild impacts (which showed little surface damage after impaction, per visualization with India ink, Fig. 2B), moderate and severe impacts visibly deformed the surface of the articular cartilage, which we had hypothesized would significantly compromise tribological rehydration. Impacts of the severities investigated in this study caused damage to the cartilage surface, however this damage was confined to entirely within the cSCA contact area and did not visibly penetrate to the subchondral bone, potentially allowing for the cartilage contact to remain 'fully sealed' against the glass slide during reciprocation. This sealing effect may enable the retention of the hydrodynamic environment necessary for sustaining tribological rehydration in the cSCA after our impacts were delivered.

These results suggest that following impact, physical wear might be a secondary driver of cartilage degeneration and PTOA development, with impact-induced cellular dysfunction potentially driving cell-mediated matrix remodeling, catabolism, and tissue degeneration instead (Jeffrey et al., 1995; Torzilli et al., 1999; Chen et al., 2001). It is well established that high-stress impacts can cause acute chondrocyte dysfunction and death (Chen et al., 2001), leading to altered matrix homeostasis (increased catabolism) (Torzilli et al., 1999) and biomechanical properties (Jeffrey and Aspden, 2006). However, because our cartilage samples had been previously frozen and stored with protease inhibitors, we assumed the cartilage to be 'acellular' and minimally affected by matrix metalloproteinase activity following injury. Repeating this study with live (viable) tissue and extended explant culture after impaction could help elucidate the role that impact-induced and cell-mediated ECM degradation has on cartilage homeostasis, composition, and permeability post-impaction (Ewers et al., 2001; Buckwalter, 2002). Such studies would inform the cellular pathoetiology of impact-induced cartilage dysfunction under physiologically-consistent loading and sliding conditions, aiding in the elucidation of processes that underlie the initiation of PTOA following cartilage impact *in vivo*.

In the present study, full-thickness fissures (Section 2.3.5) and chondral defects (Section 2.3.6) altered tissue-level outcomes (i.e. cartilage's strain, strain-recovery, and friction responses) relative to their 'paired' uninjured tests. These defects are commonly observed in conjunction with joint injuries and repetitive (over-)loading activities (Bonnevie et al., 2017; Buckwalter, 2002; Repo and Finlay, 1977), and they had an appreciable influence on the immediate biomechanical and tribological rehydration responses of cartilage in the cSCA. While the biological consequence of 'injury'-induced cracks and fissures have been investigated in past studies (e.g. driving chondrocyte death, nitric oxide production, and GAG loss) (Ewers et al., 2001), the influence of such defects on the biomechanical competency of cartilage under physiological loading and sliding conditions (i.e. high compressive stresses and sliding speeds; low tissue strains and frictions) had not been previously assessed. Although not directly tested in this study, we suspect that in the cSCA configuration, full-thickness fissures and defects likely disrupt the hydrodynamic environment of the tissue, creating new flow pathways through the cartilage and altering sliding-induced tribological rehydration by providing a shorter path for depressurizing fluid flows. These new pathways promote increased start- and end-of-sliding strains, decreased strain recovery, and as a consequence, increased time-averaged strains. These findings agree with *in vivo* findings of altered strain and increased friction after cartilage injury (Ewers et al., 2001; Henao-Murillo et al., 2018; Bonnevie et al., 2018; Venalainen et al., 2016), and highlight how defects can drastically and immediately alter tribological rehydration, interstitial lubrication, and the strain and shear responses of articular cartilage. Nonetheless, tribological rehydration was not completely abolished by full-thickness injuries, as some samples exhibited a positive strain recovery following injury (Figs. 7B and 8B). However, the balance between tissue rehydration and fluid exudation clearly shifted towards that of exudation, possibly resulting from the fact that the full-thickness injuries extended down to the subchondral bone, and in the case of the fissures, beyond the edge of the contact area, causing a loss of the 'sealing effect' necessary for maintaining high rates of tribological rehydration and interstitial pressurization.

By leveraging the cSCA configuration, this study was the first to investigate the tribomechanical response of cartilage to injury under physiologically-consistent strains, stresses, sliding speeds, fluid load fractions, and friction coefficients, but it was not without limitations. Our testing setup is highly idealized in that we only applied simple reciprocation under constant compression; joint motion is complex, containing rolling and migrating contacts in addition to dynamic compression and sliding. However, the cSCA configuration allowed us to isolate and study the influence of sliding alone on the biomechanical/tribological performance of injured cartilage, without having to contend with the confounding factors of contact migration, bath exposure, and dynamic loading and unloading (Burris and Moore, 2017). Presently, we restricted our injurious impacts to locations well within the contact region between the cartilage surface and reciprocating glass slide, likely limiting the influence of 'edge effects' and loss of 'sealing' between the area of impaction and area of hydrodynamic pressurization on tribological rehydration. Future studies can address if impact location or size have differential effects on cSCA cartilage function. Our linear fissures and chondral defects were applied with sharp blades, causing 'neat' and idealized injuries which may minimize the influence of more complex fissure properties on the response of the explants to sliding. The use of somewhat small sample sizes also represents a study limitation, with many of our results exhibiting trends falling just short of significance. However, despite the small sample size, the relationships observed were clear and intuitive. Future studies will leverage the unique attributes of the cSCA explant testing configuration and the differential response of injured articular cartilage to sliding articulation to investigate how cartilage injury influences the mechanobiology of chondrocytes in live, metabolically-active tissue. Such studies will help to establish if the re-discovered cSCA testing configuration can be used to derive clinically-informative knowledge regarding the effect of joint activity/articulation on cartilage health and homeostasis following acute cartilage injury.

5. Conclusions

In summary, this investigation represents the first to directly measure strain and friction outcomes in injured cartilage explants under *ex vivo* testing conditions that replicate physiologically-relevant reciprocal sliding speeds (80 mm/s) (Moore and Burris, 2017; Graham et al., 2017b), loading magnitudes (~0.3 MPa) (Brand, 2005), and fluid load support (Burris and Moore, 2017; Moore and Burris, 2017; Graham et al., 2017a), while maintaining physiologically-consistent biomechanical and tribological outcomes (i.e. positive strain recovery and low coefficients of kinetic friction). Using the newly re-discovered cSCA explant testing configuration (Burris and Moore, 2017; Graham et al., 2017a), we demonstrated high-speed sliding can consistently and

reliably promote tribological rehydration in healthy articular cartilage, allowing for the recovery of load-induced tissue deformations and strains (Burris and Moore, 2017; Moore and Burris, 2017) that could compromise cartilage function (Krishnan et al., 2004). We also demonstrated that the immediate effects of physical cartilage injuries on tribological rehydration and biomechanical/tribological outcomes are injury type/mechanism-dependent. Full-thickness injuries such as fissures and chondral defects can markedly and immediately suppress sliding-driven tribological rehydration in cSCA explants, leading to greater cartilage strains and friction, which has the potential to promote immediate and rapid physical tissue wear and drive PTOA initiation and progression. In contrast, injurious impacts to cSCA explants had remarkably little effect on the immediate biomechanical and tribological response of cartilage to sliding, suggesting a potentially more complex etiology to impact-induced PTOA than just physical tissue wear.

Declarations of interest

None.

Funding

This material is based upon work supported by the National Science Foundation (NSF) Biomaterials and Mechanobiology program [1635536] and the NSF Graduate Research Fellowship Program [1247394]. Any opinions, findings, and conclusions or recommendations expressed in this material are those of the authors and do not necessarily reflect the views of the National Science Foundation.

Declarations of interest

None.

Acknowledgements

Thank you to Brian Graham for assisting with data analysis and Lindsay Erndwein for artistic assistance in the preparation of this publication.

Appendix A. Supplementary data

Supplementary data to this article can be found online at https://doi.org/10.1016/j.jmbbm.2019.103422.

References

Abusara, Z., Seerattan, R., Leumann, A., Thompson, R., Herzog, W., 2011. A novel method for determining articular cartilage chondrocyte mechanics in vivo. J. Biomech. 44 (5), 930–934. https://doi.org/10.1016/j.jbiomech.2010.11.031.

Argatov, I., Mishuris, G., 2015. A phenomenological model of damage in articular cartilage under impact loading. Mech. Res. Commun. 69, 87–90. https://doi.org/10.1016/j.mechrescom.2015.06.013.

Ateshian, G.A., 2009. The role of interstitial fluid pressurization in articular cartilage lubrication. J. Biomech. 42, 1163–1176. https://doi.org/10.1016/j.jbiomech.2009.04.040.

Bonnevie, E.D., Delco, M.L., Galesso, D., Secchieri, C., Fortier, L.A., Bonassar, L.J., 2017. Sub-critical impact inhibits the lubricating mechanisms of articular cartilage. J. Biomech. https://doi.org/10.1016/j.jbiomech.2016.12.034.

Bonnevie, E.D., Puetzer, J.L., Bonassar, L.J., 2014. Enhanced boundary lubrication properties of engineered menisci by lubricin localization with insulin-like growth factor I treatment. J. Biomech. 47, 213–2188. https://doi.org/10.1016/j.jbiomech.2013.10.028.

Bonnevie, E.D., Delco, M.L., Fortier, L.A., Alexander, P.G., Tuan, R.S., Bonassar, L.J., 2015. Characterization of tissue response to impact loads delivered using a hand-held instrument for studying articular cartilage injury. Cartilage 6 (4), 226–232. https://doi.org/10.1177/1947603515595071.

Bonnevie, E.D., Delco, M.L., Bartell, L.R., et al., 2018. Microscale frictional strains determine chondrocyte fate in loaded cartilage. J. Biomech. 74, 72–78. https://doi.org/10.1016/j.jbiomech.2018.04.020.

Brand, R.A., 2005. Joint contact stress: a reasonable surrogate for biological processes? Iowa Orthop. J. 25, 82–94. http://www.ncbi.nlm.nih.gov/pubmed/16089079%0Ahttp://www.pubmedcentral.nih.gov/articlerender.fcgi?artid=PMC1888787.

Buckwalter, J.A., 2002. Articular cartilage injuries. Clin. Orthop. Relat. Res. 402, 21–37. https://doi.org/10.1097/01.blo.0000026073.30435.dc.

Buckwalter, J.A., Anderson, D.D., Brown, T.D., Tochigi, Y., Martin, J.A., 2013. The roles of mechanical stresses in the pathogenesis of osteoarthritis. Cartilage 4 (4), 286–294. https://doi.org/10.1177/1947603513495889.

Burris, D.L., Moore, A.C., 2017. Cartilage and joint lubrication: new insights into the role of hydrodynamics. Biotribology 12, 8–14. https://doi.org/10.1016/j.biotri.2017.09.001. September.

Burris, D., Ramsey, L., Graham, B., Price, C., Moore, A., 2019. How sliding and hydrodynamics contribute to articular cartilage fluid and lubrication recovery. Tribol. Lett. 67 (46), 1–10. https://doi.org/10.1007/s11249-019-1158-7.

Caligaris, M., Ateshian, G.A., 2008. Effects of sustained interstitial fluid pressurization under migrating contact area, and boundary lubrication by synovial fluid, on cartilage friction. Osteoarthr. Cartil. 16, 1220–1227. https://doi.org/10.1016/j.joca.2008.02.020.

Chen, C.T., Burton-Wurster, N., Borden, C., Hueffer, K., Bloom, S.E., Lust, G., 2001. Chondrocyte necrosis and apoptosis in impact damaged articular cartilage. J. Orthop. Res. 19 (4), 703–711. https://doi.org/10.1016/S0736-0266(00)00066-8.

Dabiri, Y., Li, L., 2015. Focal cartilage defect compromises fluid-pressure dependent load support in the knee joint. Int. J Numer. Method Biomed. Eng. 31 (6). https://doi.org/10.1002/cnm.2713.

Desrochers, J., Amrein, M.W., Matyas, J.R., 2013. Microscale surface friction of articular cartilage in early osteoarthritis. J. Mech. Behav. Biomed. Mater. 25, 11–22. https://doi.org/10.1016/j.jmbbm.2013.03.019.

Eckstein, F., Tieschky, M., Faber, S., Englmeier, K.H., Reiser, M., 1999. Functional analysis of articular cartilage deformation, recovery, and fluid flow following dynamic exercise in vivo. Anat. Embryol. 200 (4), 419–424. https://doi.org/10.1007/s004290050291.

Evans, R.C., Quinn, T.M., 2006. Dynamic compression augments interstitial transport of a glucose-like solute in articular cartilage. Biophys. J. 91 (4), 1541–1547. https://doi.org/10.1529/biophysj.105.080366.

Ewers, B.J., Dvoracek-Driksna, D., Orth, M.W., Haut, R.C., 2001. The extent of matrix damage and chondrocyte death in mechanically traumatized articular cartilage explants depends on rate of loading. J. Orthop. Res. 19 (5), 779–784. https://doi.org/10.1016/S0736-0266(01)00006-7.

Falah, M., Nierenberg, G., Soudry, M., Hayden, M., Volpin, G., 2010. Treatment of articular cartilage lesions of the knee. Int. Orthop. 34 (5), 621–630. https://doi.org/10.1007/s00264-010-0959-y.

Farquhar, T., Xia, Y., Mann, K., et al., 1996. Swelling and fibronectin accumulation in articular cartilage explants after cyclical impact. J. Orthop. Res. 14 (3), 417–423. https://doi.org/10.1002/jor.1100140312.

Gannon, A.R., Nagel, T., Bell, A.P., Avery, N.C., Kelly, D.J., 2015. The changing role of the superficial region in determining the dynamic compressive properties of articular cartilage during postnatal development. Osteoarthr. Cartil. 23 (6), 975–984. https://doi.org/10.1016/j.joca.2015.02.003.

Graham, B.T., Moore, A.C., Burris, D.L., Price, C., 2017a. Sliding enhances fluid and solute transport into buried articular cartilage contacts. Osteoarthr. Cartil. 1–8. https://doi.org/10.1016/j.joca.2017.08.014.

Graham, B.T., Moore, A.C., Burris, D.L., Price, C., October 2017b. Mitigating Articular Cartilage Strains through Regular Activity. BMES Annual Meeting of the BIomedical Engineering Research Society. Phoeniz, Arizona. The relevant abstract number is 2542.

Graham, B.T., Moore, A.C., Burris, D.L., Price, C., 2018. Mapping the spatiotemporal evolution of solute transport in articular cartilage explants reveals how cartilage recovers fluid within the contact area during sliding. J. Biomech. 1–6. https://doi.org/10.1016/j.jbiomech.2018.01.041.

Henao-Murillo, L., Ito, K., van Donkelaar, C.C., 2018. Collagen damage location in articular cartilage differs if damage is caused by excessive loading magnitude or rate. Ann. Biomed. Eng. 46 (4), 605–615. https://doi.org/10.1007/s10439-018-1986-x.

Huang, C.Y., Stankiewicz, A., Ateshian, G.A., Mow, V.C., 2005. Anisotropy, inhomogeneity, and tension-compression nonlinearity of human glenohumeral cartilage in finite deformation. J. Biomech. 38 (4), 799–809. https://doi.org/10.1016/j.jbiomech.2004.05.006.

Jeffrey, J.E., Aspden, R.M., 2006. The biophysical effects of a single impact load on human and bovine articular cartilage. Proc. Inst. Mech. Eng. H 220 (6), 677–686. https://doi.org/10.1243/09544119JEIM31.

Jeffrey, J., Gregory, D., Aspden, R., 1995. Matrix damage and chondrocyte viability following a single impact load on articular cartilage. Arch. Biochem. Biophys. 322 (1), 87–96. https://doi.org/10.1006/abbi.1995.1439.

Kienle, S., Boettcher, K., Wiegleb, L., et al., 2015. Comparison of friction and wear of articular cartilage on different length scales. J. Biomech. 48 (12), 3052–3058. https://doi.org/10.1016/j.jbiomech.2015.07.027.

Kleeman, R.U., Krocker, D., Cedrano, A., Tuischer, J., Duda, G.N., 2005. Altered cartilage mechanics and histology in knee osteoarthritis: relation to clinical assessment (ICRS Grade). Osteoarthr. Cartil. 13 (11), 958–963. https://doi.org/10.1016/j.joca.2005.06.008.

Krishnan, R., Kopacz, M., Ateshian, G.A., 2004. Experimental verification of the role of interstitial fluid pressurization in cartilage lubrication. J. Orthop. Res. 22 (3), 565–570. https://doi.org/10.1016/j.orthres.2003.07.002.

Lieberthal, J., Sambamurthy, N., Scanzello, C.R., 2015. Inflammation in joint injury and post-traumatic osteoarthritis. Osteoarthr. Cartil. 23 (11), 1825–1834. https://doi.org/10.1016/j.joca.2015.08.015.

Mansour, J.M., 2003. Biomechanics of cartilage. In: Kinesiology: the mechanics and pathomechanics of human movement 2. Philadelphia, PA: Lippincott Williams and

Wilkins, pp. 66–79.
McCutchen, C.W., 1962. The frictional properties of animal joints. Wear 5, 1–17.
Milentijevic, D., Rubel, I.F., Liew, A.S.L., Helfet, D.L., Torzilli, P.A., 2005. An in vivo rabbit model for cartilage trauma: a preliminary study of the influence of impact stress magnitude on chondrocyte death and matrix damage. J. Orthop. Trauma 19 (7), 466–473. https://doi.org/10.1097/01.bot.0000162768.83772.18.
Moore, A.C., Burris, D.L., 2015. Tribological and material properties for cartilage of and throughout the bovine stifle: support for the altered joint kinematics hypothesis of osteoarthritis. Osteoarthr. Cartil. 23 (1), 161–169. https://doi.org/10.1016/j.joca.2014.09.021.
Moore, A.C., Burris, D.L., 2017. Tribological rehydration of cartilage and its potential role in preserving joint health. Osteoarthr. Cartil. 25 (1), 99–107. https://doi.org/10.1016/j.joca.2016.09.018.
Mow, V.C., Gu, W.Y., Chen, F.H., 2005. Structure and function of articular cartilage and meniscus. In: Basic Orthopaedic Biomechanics and Mechanobiology, pp. 181–258.
Patwari, P., Fay, J., Cook, M.N., et al., 2001. In vitro models for investigation of the effects of acute mechanical injury on cartilage. Clin. Orthop. Relat. Res. 391S, S61–S71.
Pawaskar, S.S., Jin, Z.M., Fisher, J., 2007. Modelling of fluid support inside articular cartilage during sliding. Proc. Inst. Mech. Eng. J J. Eng. Tribol. 221 (J3), 165–174. https://doi.org/10.1243/13506501JET241.
Punzi, L., Galozzi, P., Luisetto, R., et al., 2016. Post-traumatic arthritis: overview on pathogenic mechanisms and role of inflammation. RMD Open 2 (2), 1–9. https://doi.org/10.1136/rmdopen-2016-000279.
Rajan, V., Caligaris, M., Hung, C.T., Ahmad, C.S., Ateshian, G.A., 2010. Hemiarthroplasties defeat interstitial fluid pressurization in cartilage and promote greater friction than natural joints. Annu. Meet. Orthop. Res. Soc. 2120.
Repo, R.U., Finlay, J.B., 1977. Survival of articular cartilage after controlled impact. J. Bone. Joint. Surg. Am. 59 (8), 1068–1076. http://www.ncbi.nlm.nih.gov/pubmed/591538.
Robinson, D.L., Kersh, M.E., Walsh, N.C., Ackland, D.C., de Steiger, R.N., Pandy, M.G., 2016. Mechanical properties of normal and osteoarthritic human articular cartilage. J. Mech. Behav. Biomed. Mater. 61, 96–109. https://doi.org/10.1016/j.jmbbm.2016.01.015.
Torzilli, P.A., Grigiene, R., Borrelli, J., Helfet Jr., D.L., J, B., 1999. Effect of impact load on articular cartilage: cell metabolism and viability, and matrix water content. J. Biomech. Eng. 121 (5), 433–441. https://doi.org/10.1115/1.2835070.
Trevino, R.L., Pacione, C.A., Malfait, A.M., Chubinskaya, S., Wimmer, M.A., 2017. Development of a cartilage shear-damage model to investigate the impact of surface injury on chondrocytes and extracellular matrix wear. Cartilage 8 (4), 444–455. https://doi.org/10.1177/1947603516681133.
Venalainen, M.S., Mononen, M.E., Salo, J., et al., 2016. Quantitative evaluation of the mechanical risks caused by focal cartilage defects in the knee. Sci. Rep. 6, 1–11. https://doi.org/10.1038/srep37538. November.
Whittaker, J.L., Woodhouse, L.J., Nettel-Aguirre, A., Emery, C.A., 2015. Outcomes associated with early post-traumatic osteoarthritis and other negative health consequences 3-10 years following knee joint injury in youth sport. Osteoarthr. Cartil. 23 (7), 1122–1129. https://doi.org/10.1016/j.joca.2015.02.021.